JOURNAL OF AIRCRAFT
Vol. 42, No. 1, January–February 2005

Design of an Aerolevitation Electric Vehicle for High-Speed Ground Transportation System

Cheolheui Han* and Jinsoo Cho†
Hanyang University, Seoul 133-791, Republic of Korea
Youngjune Moon‡
Korea University, Seoul 133-791, Republic of Korea
Yonghyun Yoon§
Korea Airforce Academy, Chungwon 363-840, Republic of Korea
and
Yongkyu Song¶
Hankuk Aviation University, Seoul 412-791, Republic of Korea

An aerolevitation electric vehicle, acting as a tracked wing-in-ground-effect vehicle, is conceptually designed to match the design requirements. The aerodynamic interaction between the vehicle and its track is investigated using a combination of approaches. A boundary-element method is used to study the effect of steady, nonplanar ground effect on the vehicle. The more complicated flow characteristics are investigated using a Navier–Stokes computation. The data obtained from the numerical simulations are compared with the data measured from wind-tunnel tests. The results computed using the boundary-element method agree with the measured data. The longitudinal and lateral stability derivatives are estimated, and a guidance and control system is designed using intelligent techniques based on the estimated stability derivates.

Nomenclature

AR	=	aspect ratio
b	=	span
C_L	=	lift coefficient
C_{LF}	=	lift coefficient of a front wing
C_{LR}	=	lift coefficient of a rear wing
C_{LT}	=	lift coefficient of an aerolevitation electric vehicle
Cm	=	pitching-moment coefficient
C_p	=	pressure coefficient
Crh	=	rear wing's root chord
Crw	=	front wing's root chord
Cth	=	rear wing's tip chord
Ctw	=	front wing's tip chord
CY	=	side-force coefficient
c	=	chord length
H	=	height of wind-tunnel's test section
h	=	distance between the front wing's trailing edge and the ground
h/c	=	distance between the front wing's trailing edge and the ground divided by the front wing's root chord
hz/c	=	distance between the front wing endplate's trailing edge and the sidewall divided by the front wing's root chord
M	=	Mach number
N_{Re}	=	Reynolds number
W	=	width of wind-tunnel's test section
α	=	angle of attack
δ	=	flap deflection angle
Δx	=	distance between front wing's trailing edge and rear wing's leading edge
Φ	=	velocity potential

Presented as Paper 2002-5829 at the Design of an Aero-levitation Electric Vehicle for the High-Speed Ground Transportation System, Los Angeles Convention Center, CA, 1 October 2002; received 16 October 2002; revision received 19 March 2004; accepted for publication 19 April 2004.

*Graduate Student, School of Mechanical Engineering. Member AIAA.
†Professor, School of Mechanical Engineering. Member AIAA.
‡Professor, Department of Mechanical Engineering. Member AIAA.
§Professor, Department of Aerospace Engineering. Member AIAA.
¶Professor, Department of Aeronautical and Mechanical Engineering. Member AIAA.

I. Introduction

ENVIRONMENTAL problems, such as the greenhouse effect and the production of human genetics damaging teratogenic constituents, have been serious issues all over the world. A cause of these environmental problems is the enormous amount of energy required by modern civilization for transportation purposes. This problem could be reduced with the development of a high-speed ground transportation system that utilizes a new concept vehicle. The new concept vehicle must be able to move faster and consume less energy than current vehicles.

In recent years, a high-speed guideway train (Aero-Train)[1] has been proposed in Japan. The Aero-Train concept uses solar energy as a power source[2] and is therefore considered a "zero-emission vehicle." Drastic drag reduction is obtained by utilizing the wing-in-ground (WIG) effect. In Korea, an aerolevitation electric vehicle (AEV)[3–6] has been proposed as a novel form of ground transportation. The AEV is an over-the-ground-surface tracked wing inground effect vehicle (TWIG).[7,8] The TWIG is a tracked overland vehicle that flies in close proximity to the ground, achieving its guidance and levitation from aerodynamic forces. The AEV is propelled by counter-rotating propellers using electricity as a power source.

Since Wieselsberger[9] first applied the method of images to satisfy the no-penetration boundary condition on the ground, there has been a wide spectrum of numerical approaches used to calculate the aerodynamic properties of objects in ground effect. These approaches range from simple lifting-line methods to complicated computational-fluid-dynamic analyses. Ollia[10] and Hooker[11] published historical reviews of WIG vehicles and discussed some of the technological information necessary to develop these vehicles. Rozhdestvensky[12] presented an extensive literature review on WIG development.

Early studies on the WIG effect were analytic. Tomotika et al.[13] and Havelock[14] used conformal mapping to find exact solutions for the flow around an airfoil near the ground. Rozhdestvensky[12]

presented mathematical models for the nonlinear aerodynamics of lifting surfaces in extreme ground effect.

With the rapid increase in computing power, numerical methods based on potential flow theory have become widely used. Katz[15] used a vortex-lattice method to investigate the effect of the ground on the aerodynamic properties of race car spoilers. Nuhait and Mook[16] also developed a general model of finite lifting surfaces in steady and unsteady ground effect. Goez et al.[17] performed the aerodynamic analysis of a low-aspect-ratio rectangular wing with endplates and trailing-edge flap deflections using a PANAIR-panel method. Maskew[18] investigated the ground effect for a wing with various aspect ratios to validate the low-order panel method code, VSAERO. Chun and Park[19] performed steady and unsteady aerodynamic calculations to investigate the WIG effect on wings moving near the surface of water. They showed that the ground effect for a wing above waves is lower than that for a wing above flat ground. Mizutani and Kazuo[20] calculated the effect of thickness for a wing moving near the ground. Navier–Stokes codes have started to be used in the aerodynamic analysis of wings in ground effect. Recently, Hirata and Kodama[21] applied a Navier–Stokes solver to study the ground effect of a three-dimensional wing with endplates.

Fink and Lastinger[22] performed an experimental study of ground effect by placing two airfoils symmetrically in a wind tunnel to imitate the method of images. This method eliminated the unrealistic boundary layer that is present on the ground with the wing and ground-board method. Binder[23] presented the experimental

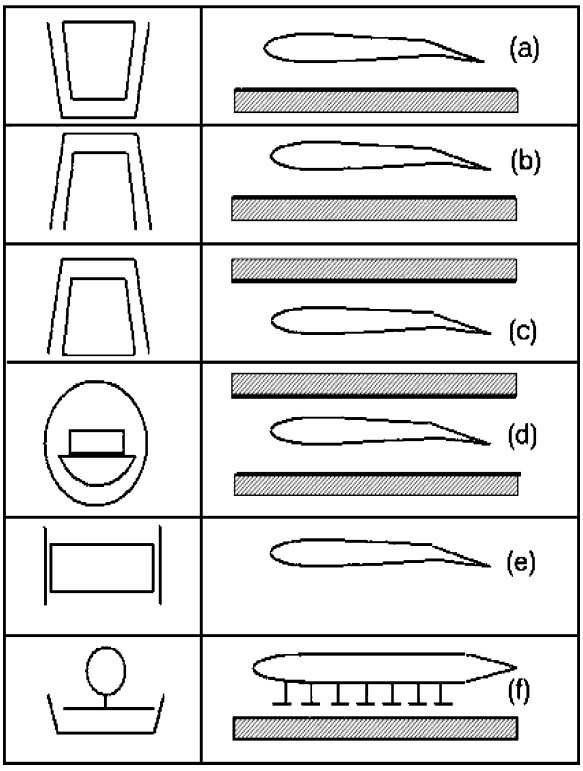

Fig. 1 Lift mechanism and guide way concepts.[8]

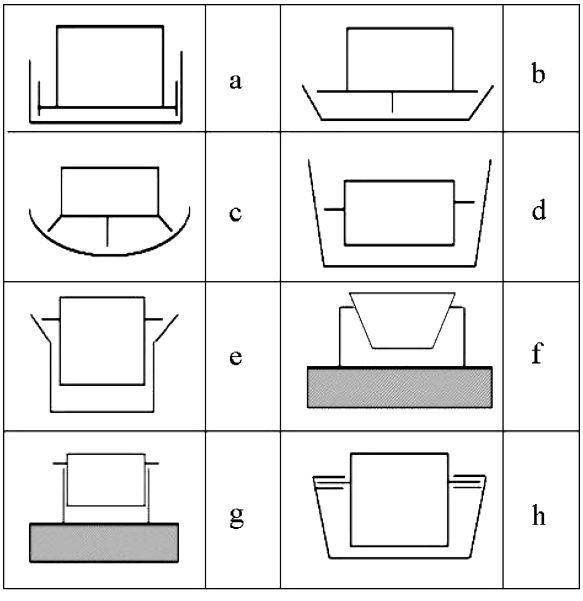

Fig. 2 Cross-section concepts.[8]

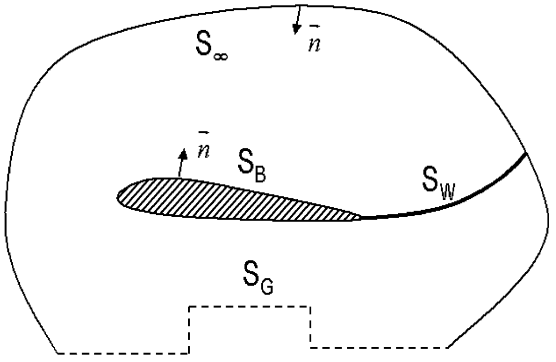

Fig. 3 Flow domain and boundaries.

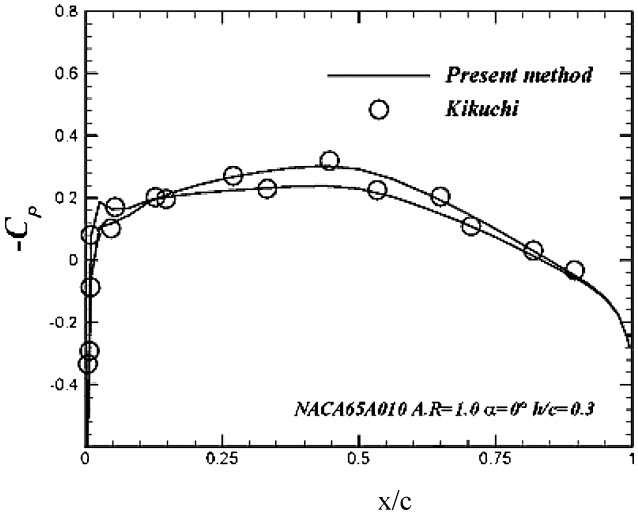

a) $\alpha = 0$ deg

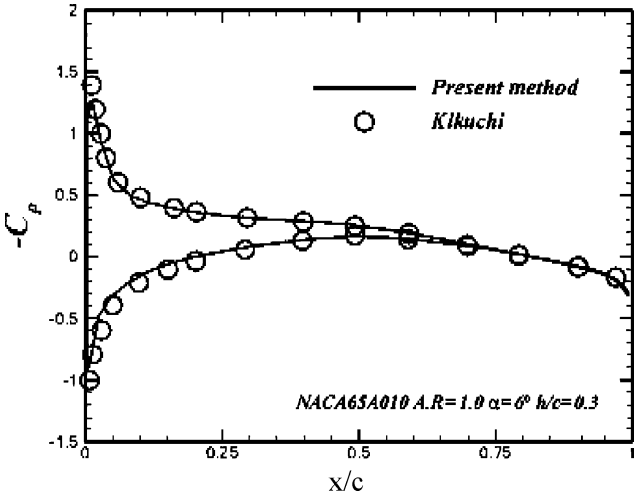

b) $\alpha = 6$ deg

Fig. 4 Pressure coefficient values over a NACA wing at $h/c = 0.3$.

results for wings with AR = 2.8, $h/c = 0.6$ and AR = 7, $h/c = 1.5$. Chang,[24] Chang and Muirhead,[25] and Lee et al.[26] investigated the static and dynamic ground effect of low-aspect-ratio wings by using the ground-board method. These experimental studies have difficulty in simulating the ground moving with vehicles. Also, their cost is large compared to other analytic or numerical methods. Zhang and Zerihan[27] investigated a cambered, double-element, high-lift wing operating in ground effect. They showed that boundary-layer separation, and the resultant loss of circulation on the main element, causes a sharp reduction in the downforce on a wing with a large flap angle.

Mithra[8] developed a simple methodology for the aerodynamic, dynamic, and economic analysis and evaluation of the TWIG. His main study is focused on roadable cars or buses. He evaluated the TWIG by comparing it with other tracked air cushion vehicle[28] and magnetically levitated vehicles.[29] So far, only a limited amount of research has been done on TWIG vehicles, with significant attention being directed toward over-the-sea WIG vehicles over the last three decades. To design the TWIG vehicles at an initial conceptual aerodynamic design level, it should be possible to calculate the aerodynamic characteristics of wings moving in a track as quickly as possible.

A boundary-element method based on potential flow theory is developed to predict the aerodynamic characteristics of wings flying over a nonplanar track. The conceptual aerodynamic design of the AEV is performed using this boundary-element method. The aerodynamic interaction of the AEV with its guideway is investigated with both the boundary-element method and turbulent viscous flow computations. Wind-tunnel tests are performed with a 1/20th-scale test model. The longitudinal and lateral aerodynamic derivatives are estimated based on the designed aerodynamic coefficients with the help of conventional aircraft design tools.

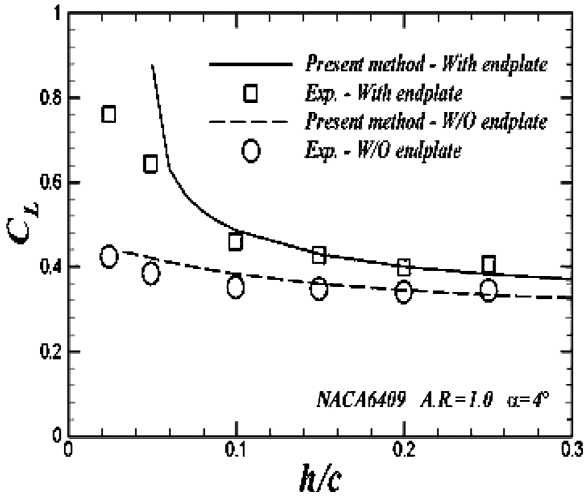

Fig. 5 Lift coefficient variation of a NACA 6409 wing with an aspect ratio of one and at an angle of attack of 4 deg.

II. Boundary-Element Method

The flow is assumed to be inviscid, incompressible, and irrotational over the entire flow-field, excluding the wing's solid boundaries and its wake. Therefore a velocity potential $\Phi(X, Y, Z)$ can be defined, and the continuity equation becomes Laplace's equation:

$$\nabla^2 \Phi = 0 \tag{1}$$

Consider a body with known boundaries S_B (wing surface), S_W (wake surface), S_G (ground surface), and S_∞ (outer boundary) as shown in Fig. 1. The general solution to Eq. (1) can be constructed, based on Green's identity, by a sum of source σ and dipole μ distributions on all of the boundaries:

$$\Phi(x, y, z) = \frac{1}{4\pi} \int_{S_B + S_W + S_G} \mu \boldsymbol{n} \cdot \nabla \left(\frac{1}{r} \right) \mathrm{d}S - \frac{1}{4\pi} \int_{S_B + S_G} \sigma \left(\frac{1}{r} \right) \mathrm{d}S + \Phi_\infty \tag{2}$$

To impose the Dirichlet boundary condition on the surface, the perturbation potential has to be specified everywhere on S_B. If for

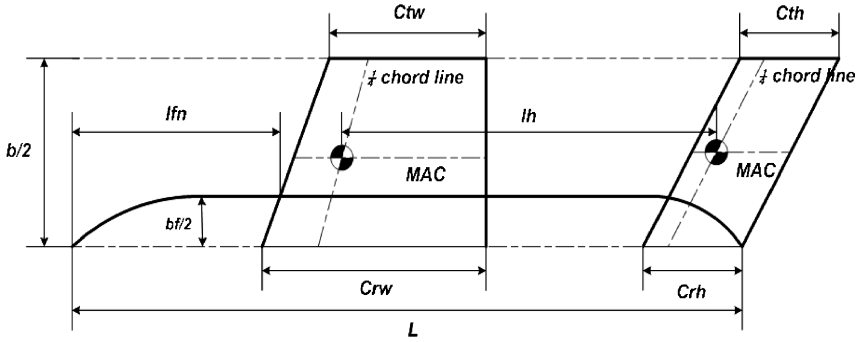

Fig. 6 Nomenclature used for the AEV design.

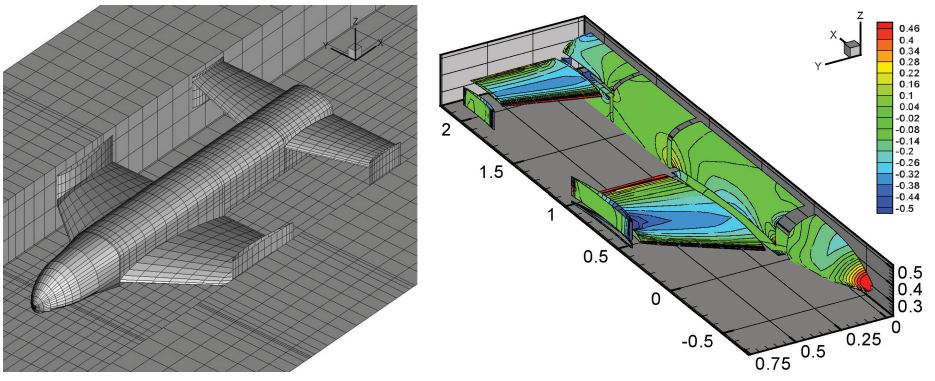

Fig. 7 Example of surface-panel distributions over AEV I and resultant pressure coefficient contours.

an enclosed body $\partial\Phi/\partial n = 0$, then the potential inside the body will not change. Thus, Eq. (2) becomes

$$\Phi_i(x, y, z) = \frac{1}{4\pi}\int_{S_B+S_W+S_G} \mu \boldsymbol{n}\cdot\nabla\left(\frac{1}{r}\right)\mathrm{d}S$$

$$-\frac{1}{4\pi}\int_{S_B+S_G}\sigma\left(\frac{1}{r}\right)\mathrm{d}S + \Phi_\infty = \text{const} = \Phi_\infty \tag{3}$$

Equation (3) can then be reduced to the following form:

$$\int_{S_B+S_W+S_G}\mu\boldsymbol{n}\cdot\nabla\left(\frac{1}{r}\right)\mathrm{d}S - \int_{S_B+S_G}\sigma\left(\frac{1}{r}\right)\mathrm{d}S = 0 \tag{4}$$

To find the unique solutions of Eq. (4), the following conditions must be satisfied:

1) The flow disturbance, caused by the wing's motion through the fluid, should vanish far from the wing. This boundary condition can be satisfied automatically by specifying sources and dipoles as singularity distributions.

2) The normal flow through solid boundaries must be zero.

$$(\nabla\Phi)\cdot\boldsymbol{n} = 0 \tag{5}$$

where $\boldsymbol{n}$ is the normal to the body's surface. The Dirichlet boundary condition requires that the source strength be given as follows:

$$\sigma = -\boldsymbol{n}\cdot(\boldsymbol{V}_0) \tag{6}$$

The geometry of the body is divided into surface-panel elements. For each panel, the corner points, collocation points, and outward normal vectors are identified. The specification of the Dirichlet boundary condition at the ith panel's collocation point, with the N wing and ground surface panels and Nw wake panels, will have the form as follows:

$$\sum_{k=1}^{N} C_{ik}\mu_k + \sum_{l=1}^{Nw} C_{il}\mu_l + \sum_{k=1}^{N} B_{ik}\sigma_k = 0 \tag{7}$$

where k is the counter for the wing and the ground surface panels and l is the counter for each panel on wake surface.

3) The Kutta condition is satisfied by specifying the strengths of doublets at the trailing edge as zero.

The unknown strengths of the potentials are determined by inverting the aerodynamic influence coefficient matrices. The surface velocities over the wing surfaces are obtained using the potential

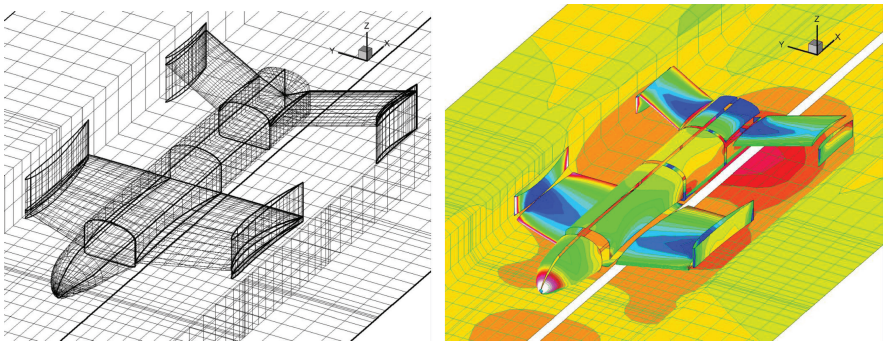

Fig. 8 Example of surface-panel distributions over AEV II and resultant pressure coefficient contours.

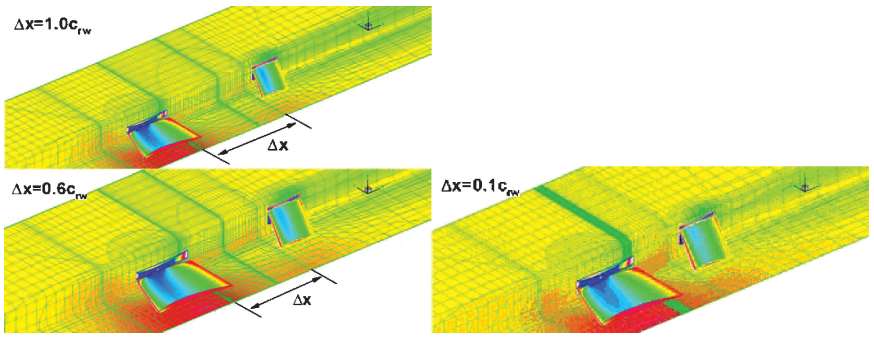

a) Pressure coefficient contours

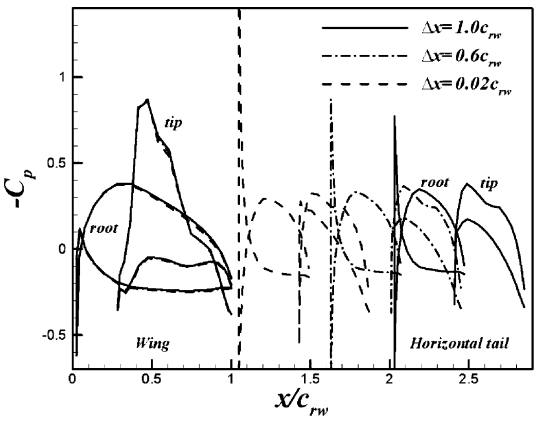

b) Pressure coefficient

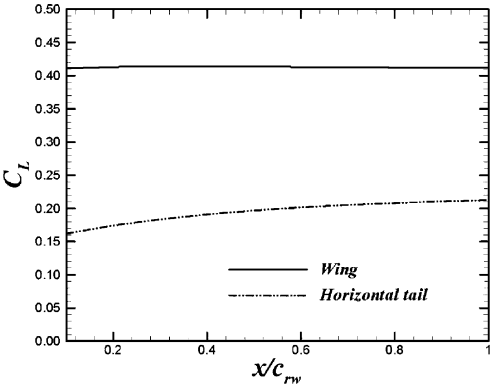

c) Lift coefficient

Fig. 9 Aerodynamic characteristics of AEV wings ($h/C_{rw} = 0.2$, $h/C_{tw} = 0.213$, $h/C_{rh} = 0.858$).

strengths, and the surface static pressures are calculated from Bernouilli's equation. The net aerodynamic forces on the wing are calculated by integrating the pressure values over the wing's surface.

III. Aerodynamic Design of AEV Considering Its Aerodynamic Interaction with Channel-Type Guideway

Multidisciplinary studies on the development of a next-generation high-speed ground transportation system (HGTS) using an AEV (AEV-HGTS) followed two consecutive research stages. The first stage consisted of determining preliminary vehicle configurations by ignoring the vehicle's aerodynamic interaction with the guideway.[3,4,7] It is known that the aerodynamic interaction of the AEV with the guideway can affect the aerodynamic characteristics of the AEV. Thus, the second stage consisted of determining the aerodynamic interaction between the AEV and its guideway. This ensured that the preconfigured AEV could operate safely over the guideway therefore satisfying the design requirements.[5–7]

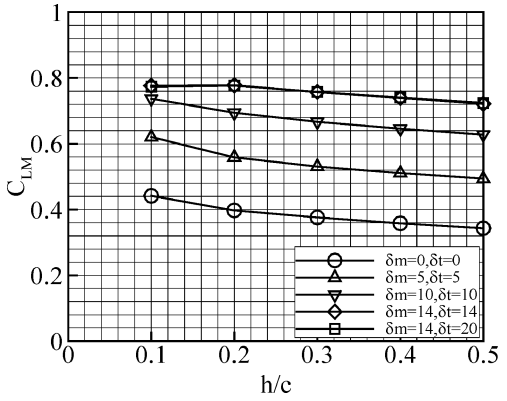

a) Front wing

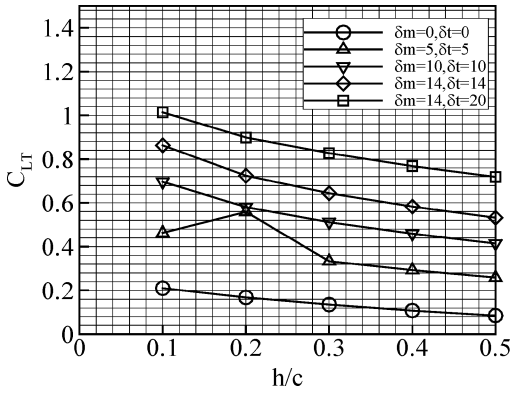

b) Rear wing

Fig. 10 Lift coefficient variations of AEV wings for the change of ground height and flap deflection angle.

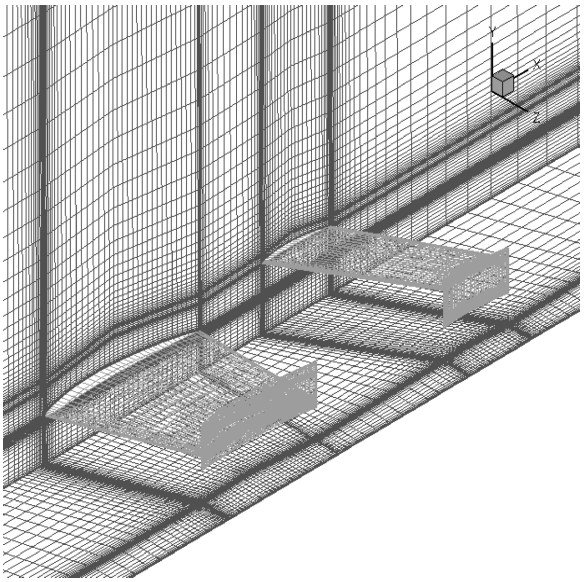

Fig. 11 Grid for the AEV-guideway interaction.

A. Conceptual Design of the Guideway

Figure 2 shows the possible lift mechanism and guideway concepts. From the definition of the AEV, consideration was limited to fluid dynamic lift mechanisms, that is, a powered air cushion and magnetic levitation were not included. Figure 3 shows the various cross-section concepts. The lift mechanism and cross-section geometry of the HGTS were selected based on published literature.[8] The authors determined that the fence-type guideway was an optimal choice for the AEV's safe operation with low construction costs. The fence has the following advantages[8]: 1) this configuration has statically stable heave, roll, pitch, yaw, and side-displacement aerodynamic stiffness derivatives as a result of the endplate gap effects; 2) low sidewalls permit a view to the passengers—this being a significant plus from a passenger's viewpoint; 3) relatively low guideway construction costs compared to other guide ways; and 4) the guideway is in the form of a shallow channel, thus trapping the leakage flows between the ground and the fence.

B. Aerodynamic Design of an AEV-HGTS Using a Boundary-Element Method

WIG vehicles have usually smaller wing areas compared with conventional airplanes because they utilize the ground effect.

In Fig. 4, calculated pressure coefficients over a NACA 65A10 wing with an aspect ratio of one are plotted along the midspan of the wing. The present results are compared with the results of Kikuchi.[30] The figure shows that the present results are in good agreement with Kikuchi's results.

Figure 5 shows the lift coefficient variation of a NACA 6409 wing with an aspect ratio of one and at an angle of attack of 4 deg. In the figure, present results agree well with the experimental data[30] for ground height values greater than $h/c = 0.06$. Below $h/c = 0.06$, the clearance between the endplate and the ground surface is so small that a large number of small-size panels are required to sufficiently capture the flow characteristics.

Figure 6 shows the nomenclature used for the aerodynamic design of the current AEV-HGTS. This AEV has a low wing configuration and a cabin with a rectangular cross-section bottom. The aerodynamic design was performed using the boundary-element method (BEM). The surface-panel distributions for the aerodynamic analysis of the AEV I and the calculated pressure coefficient contours are shown in Fig. 7. Table 1 shows the geometrical specifications of the AEV I. The design of AEV I was completed without considering the longitudinal stability.

The surface-panel distributions for the aerodynamic analysis of the AEV II and the calculated pressure coefficient contours are shown in Fig. 8. Table 2 shows the geometric specifications of the AEV II. The rear wing geometry was modified by using the advanced aircraft analysis (AAA). The swept-back angle of the AEV I was changed from 0 to 30 deg to move back the mean aerodynamic

Table 1 Specifications of an AEV I geometry

Design variables	Front wing	Rear wing
AR	1.757	3.386
S	128.02 m^2	66.45 m^2
b	15 m	15 m
Λ_{LE}	21.9 deg	30 deg
$\Lambda_{c/4_w}$	16.8 deg	30 deg
λ	0.70	0
c_r	10.04 m	4.43 m
c_t	7.03 m	4.43 m
$\bar{c}$	8.623 m	4.43 m

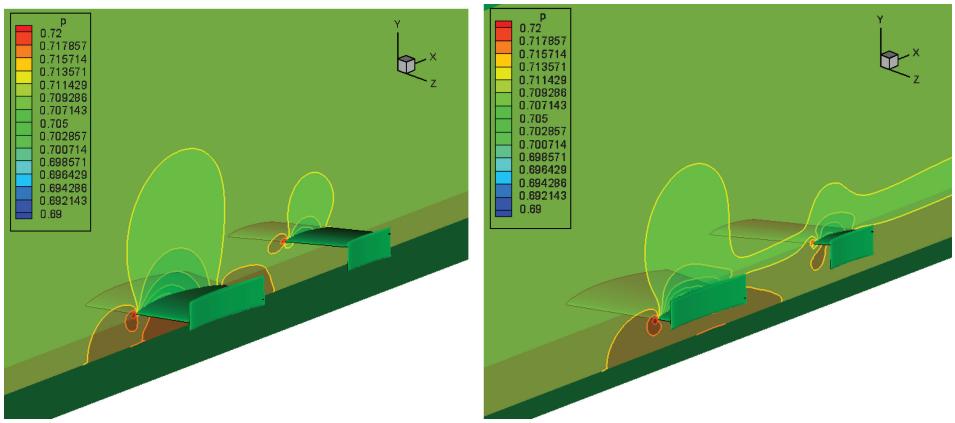

Fig. 12 Static-pressure contours at several spanwise sections ($h/c = 0.1$).

Table 2 Specifications of an AEV II geometry

Design variables	Front wing	Rear wing
AR	1.751	3.56
S	128.5 m^2	63.2 m^2
b	15 m	15 m
Λ_{LE}	39 deg	18 deg
$\Lambda_{c/4_w}$	30.3 deg	13.647 deg
λ	0.475	0.552
c_r	11.6 m	5.43 m
c_t	5.5 m	3.0 m
$\bar{c}$	8.987 m	4.33 m

Table 3 Aerodynamic coefficients of the designed AEV

Ground height (h/c)	C_L	C_D	C_L/C_D	C_Y
	Front wing			
0.1	0.59	0.0234	25.26	0.178
0.2	0.524	0.0242	21.65	0.215
	Rear wing			
0.1	0.266	0.0293	9.08	−0.233
0.2	0.214	0.03	7.13	−0.174

chord of the rear wing, which affects the tail volume coefficient. The pitching-moment curve slope $C_{M\alpha}$ for the AEV II was found to equal −0.83.

Figure 9 shows the aerodynamic characteristics of AEV wings. In Fig. 9a, the pressure coefficient contours over the wings, ground surface, and fence are plotted for several values of the gap length between the AEV wings. The pressure coefficients at the wing root and the wing tip are plotted in Fig. 9b. The lift coefficient variation of the rear wing is plotted in Fig. 9c against the length between the front wing and the rear wing. It can be concluded from these figures that the distance from the trailing edge of the AEV's front wing to the leading edge of the AEV's rear wing should be small in order to maximize the rear wing's lift.

Figure 10 shows the AEV wing's variation of lift coefficient with the change of ground height and flap deflection angle. Though not shown in Fig. 10, the maximum lift coefficients for both wings (0.77 for the front wing at a flap deflection angle of 14 deg and 1.17 for the rear wing at a flap deflection angle of 30 deg) are obtained. However, the liftoff speed is still over 200 km/h (more exactly 216 km/h for a gross takeoff weight of 40 tons). From these calculations, it was concluded that present AEV high-lift devices (i.e., conventional flaps) could not produce lift forces large enough to achieve a stable takeoff.

C. Turbulent Viscous Computation for Aerodynamics and Flow Interaction of AEV Wings with Guideway

The flow characteristics of the HGTS are complex because of the complicated geometries of the AEV and the wall effect. Turbulent viscous flow computation using the k–ε and Spalart–Allmaras

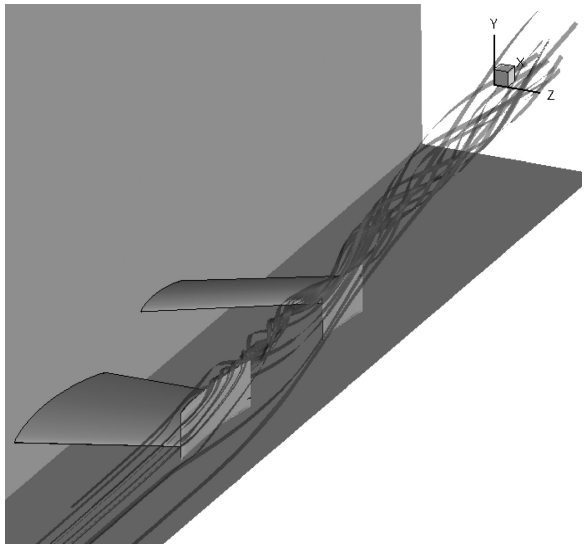

Fig. 13 Streamlines showing the tip vortex trajectories behind the endplate of the front wing.

turbulence models were performed to investigate the aerodynamic characteristics and flow interaction of the designed AEV wings with the guideway.[5,31] It was suspected that the clearance between the AEV wing's endplates and the guideway would significantly effect the AEV's aerodynamic performance. Thus, the effect of the clearance on the aerodynamic characteristics of the AEV wings was investigated as well.

Figure 11 shows the accomplished grid generation with six blocks and one million meshes. Three-dimensional steady turbulent flows were calculated using six alpha-chip CPUs and with message-passing interface passing for parallel computing. The computation was performed for the flow condition of $M = 0.2$, $N_{\mathrm{Re}} = 2 \times 10^6$, $\alpha = 2$ deg, and $h/C_{\mathrm{tw}} = 0.159$.

Figure 12 shows the static-pressure contours at several spanwise sections from the wing root to the wing tip. It is shown in the figure that the air trapped between the wing and the ground produces the highly pressurized region beneath the front wing.

The effect of tip vortices on the AEV I's rear wings is shown in Figs. 13 and 14 and Table 3. Figure 13 shows the streamlines representing tip vortex trajectories behind front wing's endplates. Tip vortices generated from the front wing's endplates move downstream and sweep through the rear wing's endplates. In Fig. 14, the static-pressure contours are plotted at several cross sections in the downstream direction. Table 3 shows that the side forces for the rear wings are negative. The rear wings are sucked into the sidewall. The tip vortices behind the front wings accelerate the flows between the endplate and the sidewall. This accelerated flows cause the endplate to suck into the sidewall.

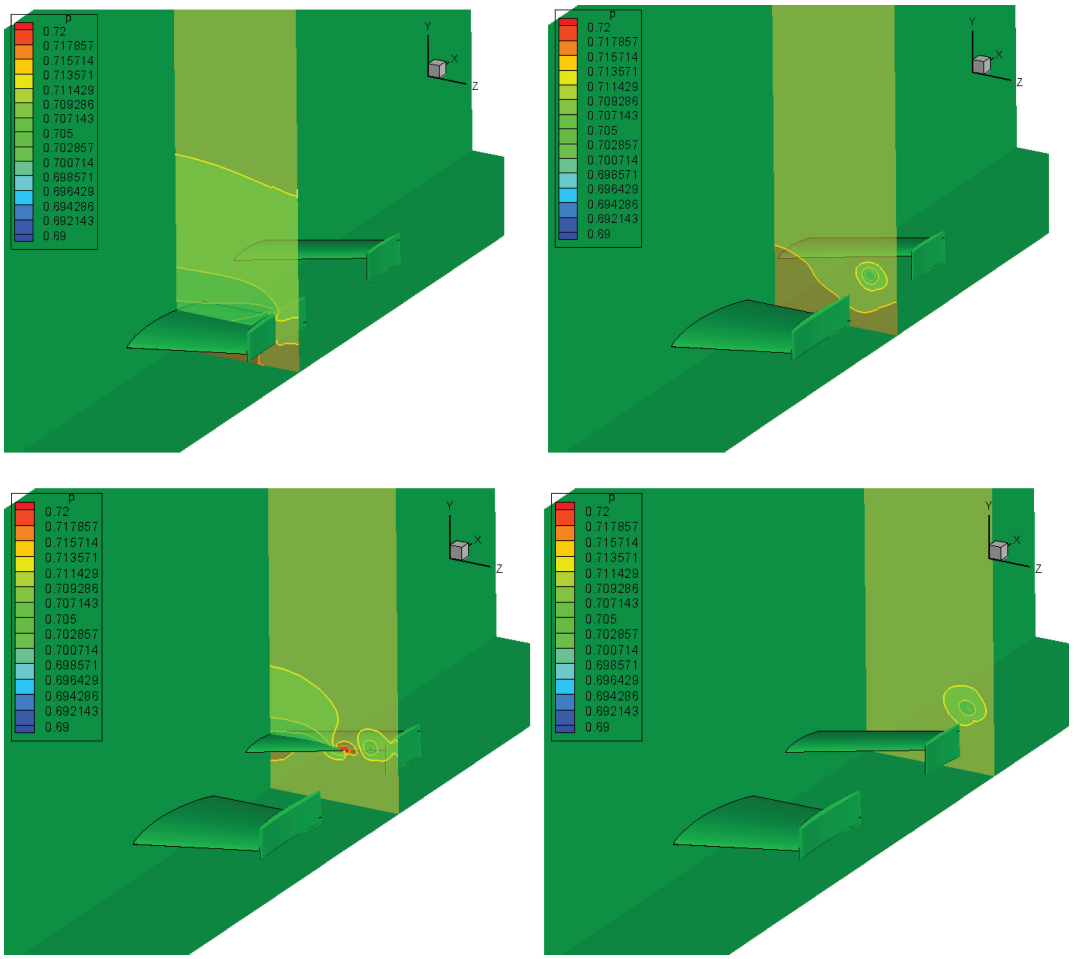

Fig. 14 Static-pressure contours at several cross sections behind the endplate of the front wing.

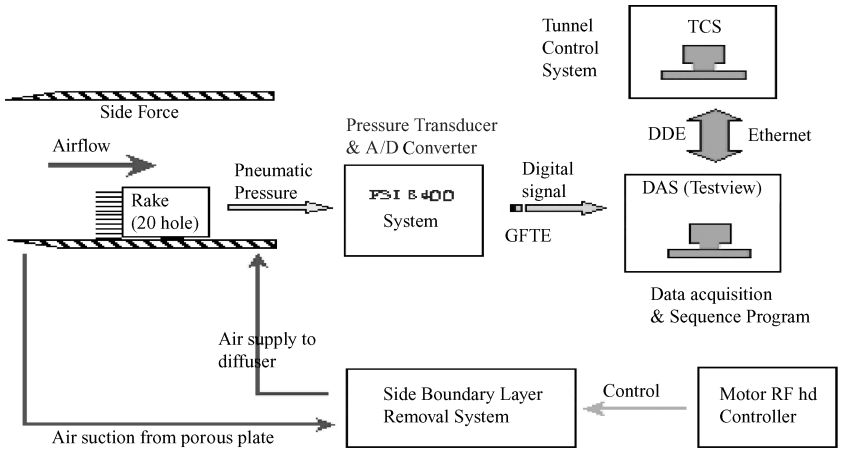

a) Sidewall

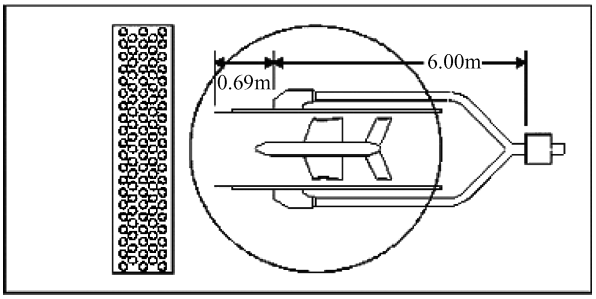

b) Ground board

Fig. 15 Boundary-layer removal system.

Table 4 shows the effect of the clearance between the front wing's endplate trailing edge and the sidewall on the lift coefficient of the front wing. As the clearance decreases, the lift increases.

D. Wind-Tunnel Test with a 1/20-Scale-Down AEV and the Guideway

Wind-tunnel tests were performed for the same flow conditions as used for the turbulent viscous calculations. These tests were carried out in a closed-circuit wind tunnel with a test section of 2.4(h) × 3.5(w) m and a section length of 8.7 m. Under these test conditions the freestream turbulence intensity was 0.076%. The lift, drag, and pitching-moment data were corrected for support tare and strut interference as determined from tare tests. The usual model blockage correction was applied to the measurements.

Figure 15 shows the test rig setup with the boundary-layer removal system (BLRS) for the ground-effect simulation. The boundary layer was sucked away through a porous plate on the bottom of the test section. The velocity reached the freestream value less than 2 mm from the ground. Repeatability was found to be excellent. It was found that the BLRS was able to reduce the displacement thickness by 70%. Using a 1/20th-scale test model and a model guideway, wind-tunnel tests were performed for various angles of attack and ground height values. Using procedures detailed in the Ref. 32, these measurements were found to have an uncertainty of 5%.

Figure 16 shows the wind-tunnel test setup with a 1/20th-scale AEV and a model guideway. Test conditions are shown in Table 5. In Table 5, EX1 represents the experiment done without sidewalls. EX2 is the experiment, which includes the BLRS, of the AEV interaction with the guideway. For EX3, the right-side endplate of the AEV wing is exchanged with a flat plate to evaluate the effect of the airfoil cross section on the aerodynamic characteristics of the endplates.

Because the AEV is guided by the guideway, it is important to investigate the effect of the guideway on the aerodynamic characteristics of the AEV.

Table 4 Aerodynamic coefficients of the AEV front wing for the clearances with the sidewall ($h/c = 0.2$)

hz/c	C_L	C_D	C_L/C_D
0.1	0.522	0.025	20.88
0.2	0.507	0.0252	20.12

Figure 17 shows the aerodynamic coefficient variations for different angles of attack and ground heights. This figure shows that the guideway increases both the lift and drag coefficients. It is seen that the guideway's effect on the pitching-moment coefficient is to create a more nose-down pitching moment. Figure 17 also shows that the effect of the flap deflection angle is to increase the lift and the longitudinal stability of the AEV while reducing the drag.

Figure 18 shows the effect of the endplate clearance from the sidewall for the front wing at $h/c = 0.2$. As shown in the figure, the small clearance increases the longitudinal stability and the lift-to-drag ratio. The side force is increased for small clearance values.

Figure 19 shows the effect of the airfoil section vs flat plate for the endplate of the AEV wings. The endplates of the AEV wings have NACA 4406 airfoil sections, which are set at an incidence angle of 2 deg. In Fig. 19, the endplates with the airfoil sections are shown to have a higher lift-to-drag ratios than the endplates with flat plate sections. Figure 19 also shows that the side forces from the endplates with the airfoil sections are larger than those with flat plates.

Tables 6 and 7 show the comparison of the computed lift coefficients by the panel method to the measured data. The

Table 6 Comparison of the computed lift coefficients by the panel method and the measured data: panel method

h/c	C_{LF}	C_{LR}	C_{LT}
0.1	0.301	0.070	0.371
0.2	0.268	0.059	0.327
0.5	0.228	0.025	0.253

Table 7 Comparison of the computed lift coefficients by the panel method and the measured data: experiment

h/c	C_{LT}	C_{DT}
0.15	0.31	0.057
0.2	0.30	0.058

Table 5 Wind-tunnel test conditions

Variables	V, m/s	α	δ	h/c	BLRS (ground)	BLRS (sidewall)	Fence clearance		Endplate w: with
EX1	——	——	——	——	ON	w/o	0.1	0.1	w
EX2		0	0	0.15	ON	ON	0.1	0.2	w
		1	10	0.20			0.1	0.3	
	34	2		0.25			0.2	0.2	
		3					0.2	0.3	
EX3	——	——	——	——	ON	ON	0.1	0.2	w
							0.1	0.3	
							0.2	0.2	
							0.2	0.3	

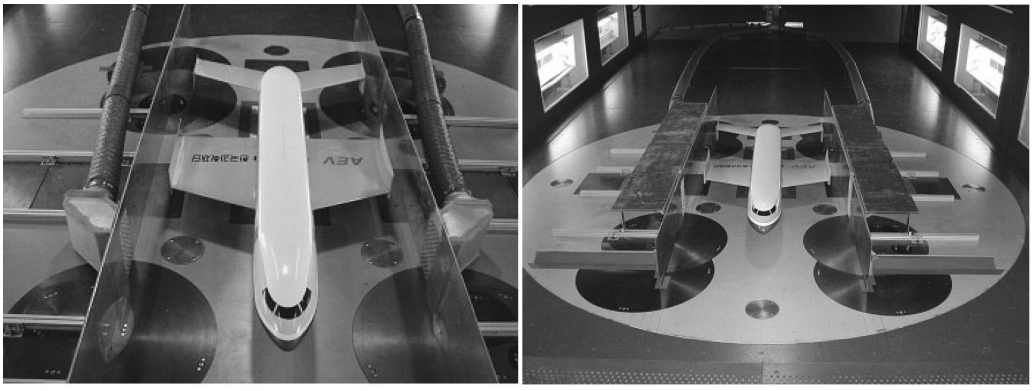

Fig. 16 Wind-tunnel test with a 1/20th-scale-down AEV and the guideway.

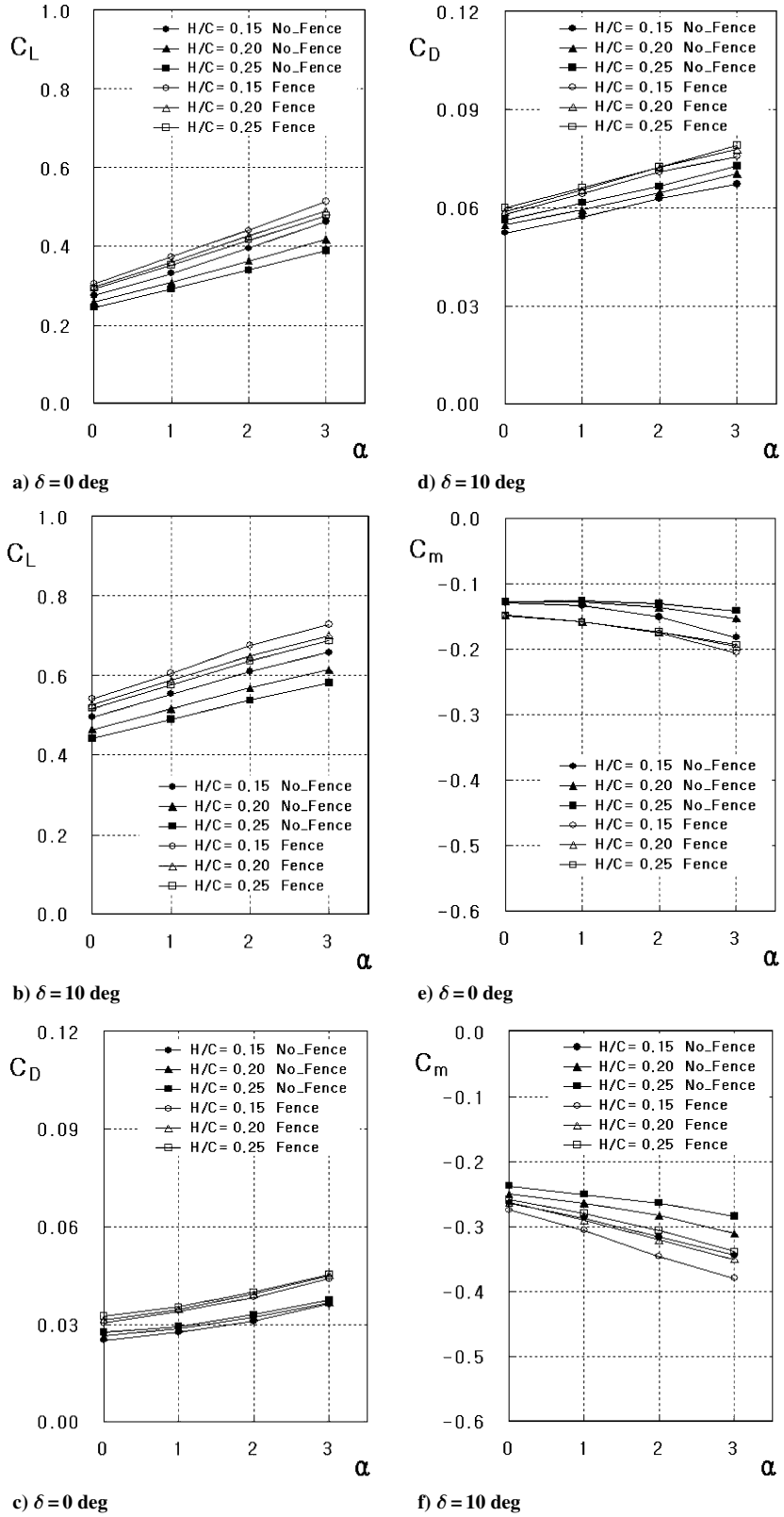

a) $\delta = 0$ deg

b) $\delta = 10$ deg

c) $\delta = 0$ deg

d) $\delta = 10$ deg

e) $\delta = 0$ deg

f) $\delta = 10$ deg

Fig. 17 Aerodynamic coefficient variations for different angles of attack and ground heights.

reference area for C_{LF}, C_{LR}, and C_{LT} is the sum of the wetted areas of the front and rear wings. When the designed AEV is at $h/c = 0.2$ from the ground, the calculated lift coefficients from the panel method are 9% larger than the test data.[7] This discrepancy between the computed results and the test data is because 1) the panel method is a numerical method based on the potential flow theory, so that the panel method does not include viscous effects generated by complicated three-dimensional geometries and complex flows and 2) the test is done with the complete ALV configuration, whereas the calculation does not include the fuselage effect.

E. Guidance and Control of the AEV

As an effort of combining aerodynamic design with flight dynamics and control, the longitudinal and lateral aerodynamic derivatives were estimated based on the designed aerodynamic coefficients with

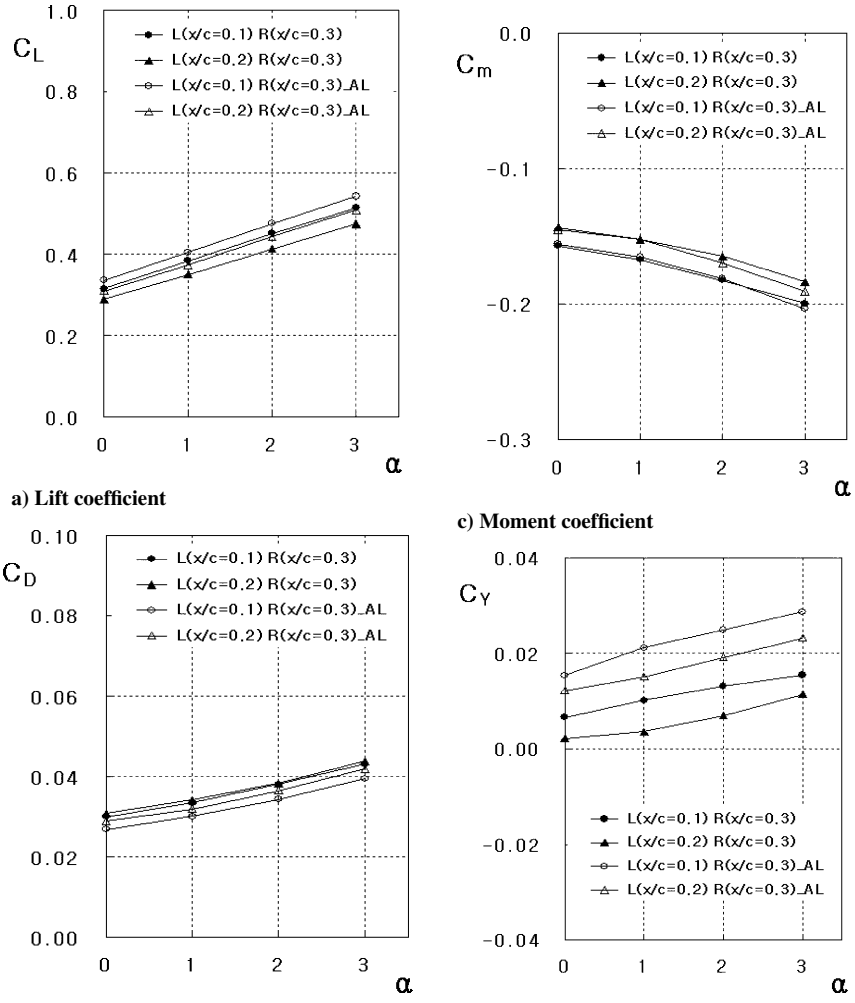

a) Lift coefficient

c) Moment coefficient

b) Drag coefficient

d) Side-force coefficient

Fig. 18 Aerodynamic coefficient variations for the change in the endplate clearance to sidewall ($h/c = 0.2$).

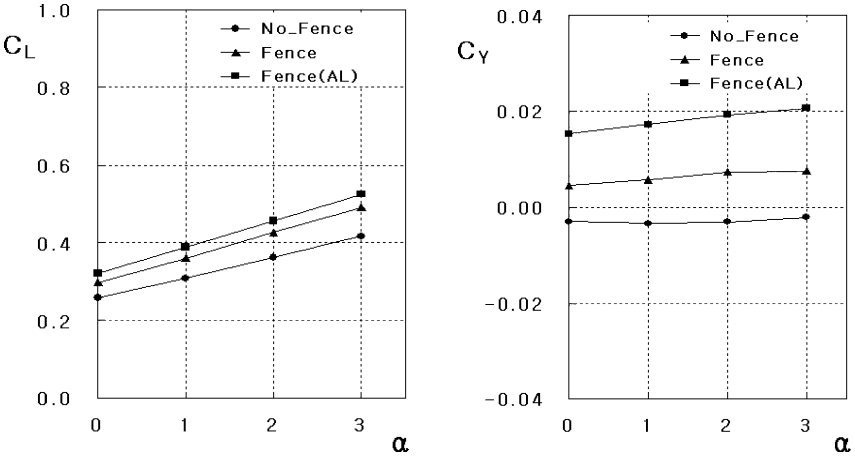

a) Lift coefficient

b) Side-force coefficient

Fig. 19 Effect of the airfoil section vs flat plate for the endplate of the AEV wings.

the help of conventional airplane design tools. Furthermore, a precision height control and guidance system was designed with the estimated derivatives. For the height control, an intelligent controller, which uses fuzzy logic with adaptation,[33] was proposed because classical control theory based on analytical methods can hardly cope with severe nonlinearities and disturbances of AEV under the close wing-in-ground effect. The fuzzy height control system takes height error and its rate as inputs and rear wing's flap deflection angles as output. Each component has seven memberships and 49 fuzzy logics. The control inputs are restricted to actuations within the given limits and rate limits. Some of simulation results are shown in Fig. 20. For the guidance and control to follow the track, a simple line-of-sight guidance was proposed to give yaw and roll commands, which were realized by using an optimal output tracking control technique.[34] Some of simulation results are shown in Fig. 21, which reveal good guidance and control.

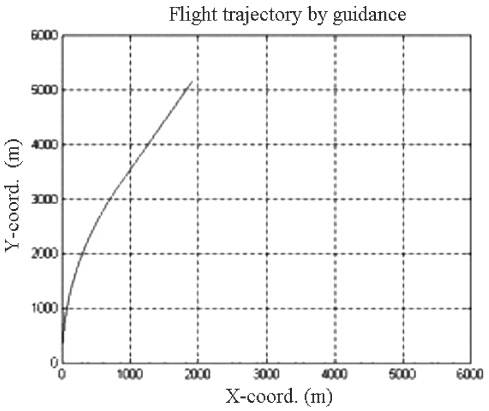

a) Flight trajectory

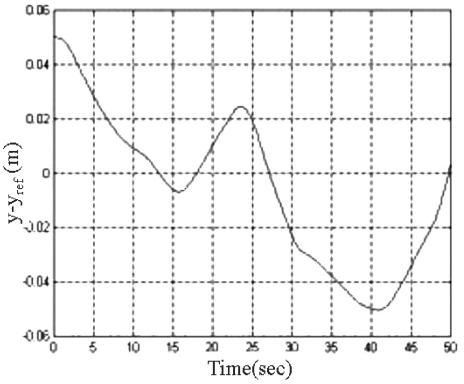

b) *y*-dir trajectory error

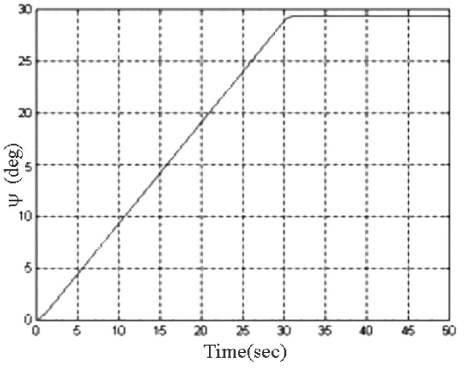

c) Yaw angle

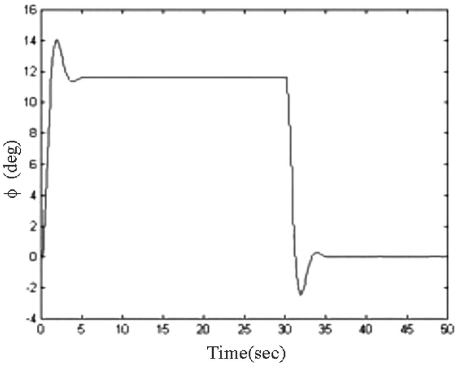

d) Roll angle

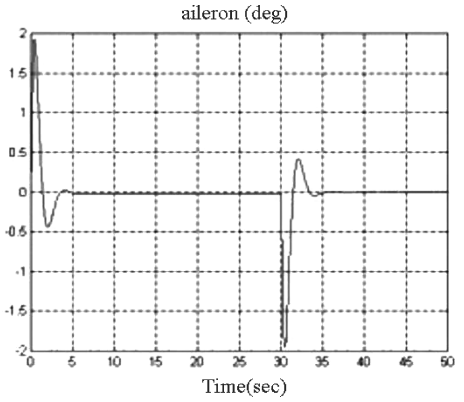

e) Aileron input

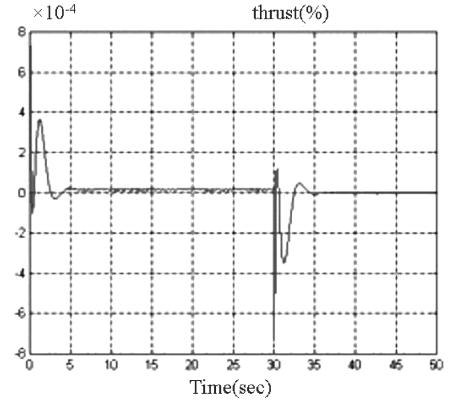

f) Thrust input

Fig. 20 Guidance and control results for the AEV II.

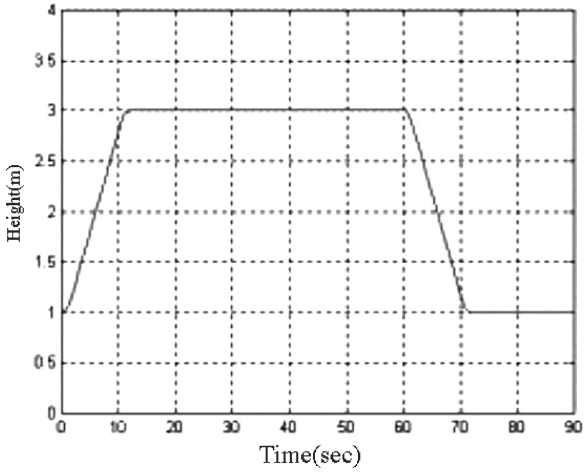

Fig. 21 Height control of the AEV.

IV. Conclusions

The aerodynamic design of a guideway was pursued so that the AEV could operate satisfying the design requirements. Through the published literature surveys, a fence-type guideway was selected as the optimal HGTS for achieving safe operation of the AEV. The configuration of the AEV for flying over the guideway was determined by using the computed results from the BEM and the aerodynamic design software, AAA. The results of the present AEV-HGTS configuration, using the turbulent viscous flow computations, showed that the tip vortex generated from the front wing's endplate affected the aerodynamics characteristics of the rear wing. The endplates of the rear wing produced the negative side forces acting towards the sidewall. This observation was used in the aerodynamic design process of the AEV-HGTS system, especially for increasing its dynamic stability. The fence guideway has the effect of increasing both the lift and the drag. The variations of the pitching-moment coefficients as a result of the changes in angles of attack and endplate clearance show the stable longitudinal stability of the AEV. For the guidance

and control of AEV, the longitudinal and lateral derivatives were estimated from the aerodynamic design of AEV, and a guidance and control system was designed based on the derivatives through the use of intelligent techniques. The simulation results show that the proposed guidance and control system is effective.

Acknowledgment

This work was supported by Grant No. (R01-1999-000-00265-0) from the Basic Research Program of the Korean Science and Engineering Foundation.

References

[1]Kono, T., Kohama, Y., and Matsui, N., "Stability of Guide Way Type Wing in Ground Effect Vehicle," *Proceedings of the Third JSME-KSME Fluids Engineering Conference*, JSME, Sendai, Japan, 25–27 July 1994, pp. 715–718.

[2]Kohama, Y. P., Kikichi, S., Watanabe, H., Ohta, F., and Ito, T., "Evaluation of the Transportation System in Relation to Environmental Problem," *Workshop on Drag Reduction of Aircraft and Ground Transportation*, Inst. of Fluid Science, Tohoku Univ., Sendai, Japan, Aug. 2000, pp. 12, 13.

[3]Cho, Jinsoo, and Han, Cheol Heui, "A Numerical Method for the Aerodynamic Design of an Aero-Levitation Electric Vehicle," *Workshop on Drag Reduction of Aircraft and Ground Transportation*, Inst. of Fluid Science, Tohoku Univ., Sendai, Japan, Aug. 2000, pp. 16, 17.

[4]Cho, Jinsoo, Han, Cheol Heui, Moon, Y., and Baek, J., "Aerodynamic Analysis and Design of an Aero-Levitation Electric Vehicle," AIAA Paper 2001-2435, June 2001.

[5]Cho, Jinsoo, Han, Cheol Heui, Moon, Y., Yoon, Y., and Song, Y., "Design of an Aero-Levitation Electric Vehicle for the High-Speed Ground Transportation System," AIAA Paper 2002-5829, Oct. 2002.

[6]Cho, Jinsoo, and Han, Cheol Heui, "Aerodynamic Analysis of Wings Flying over Nonplanar Guideways," *Proceedings of the JSASS 16th International Sessions in 40th Aircraft Symposium*, The Japan Society for Aeronautical and Space Sciences, Tokyo, Oct. 2002.

[7]Cho, Jinsoo, Han, Cheolheui, and Yoon, Yonghyun, "Aerodynamic Analysis and Design of an Aero-Levitation Vehicle for a High-Speed Ground Transportation System," AIAA Paper 2003-3505, June 2003.

[8]Sankrithi, M., "The Tracked Wing in Ground-Effect," Ph.D. Dissertation, Dept. of Mechanical and Aerospace Engineering, Princeton Univ., NJ, April 1983.

[9]Wieselsberger, C., "Wing Resistance near the Ground," NACA TM77, April 1922.

[10]Ollia, R. G., "Historical Review of WIG Vehicles," *Journal of Hydronautics*, Vol. 12, No. 3, 1980, pp. 65–76.

[11]Hooker, S. F., "A Review of Current Technical Knowledge Necessary to Develop Large Scale Wing-in-Surface Effect Craft," *Proceedings of the Intersociety Advanced Marine Vehicles Conference*, Arlington, VA, June 1989, pp. 367–429.

[12]Rozhdestvensky, K. V., *Aerodynamics of a Lifting System in Extreme Ground Effect*, Springer-Verlag, Berlin Hidelberg, 2000.

[13]Tomotika, S., Nagamiya, T., and Takenouti, Y., "The Lift on a Flat Plate Placed near a Plane Wall, with Special Reference to the Effect of Ground Upon the Lift of a Monoplane Aerofoil," Aeronautical Research Inst., Tokyo Imperial Univ., Rept. 97, Tokyo, Aug. 1933 (as reported in Pistolesi, 1935).

[14]Havelock, T. H., "The Lift and Moment on a Flat Plate in a Stream of Finite Width," *Proceedings of the Royal Society of London*, Series A, Vol. 166, No. 2, 1940, pp. 19–54.

[15]Katz, J., "Calculation of the Aerodynamic Forces on Automotive Lifting Surfaces," *Journal of Fluid Engineering*, Vol. 107, Dec. 1985, pp. 438–443.

[16]Nuhait, A. O., and Mook, D. T., "Numerical Simulation of Wings in Steady and Unsteady Ground Effects," *Journal of Aircraft*, Vol. 26, No. 12, 1989, pp. 1081–1089.

[17]Goez, A. R., Osborn, R. F., and Smith, M. L., "Wing-in-Ground Effect Aerodynamic Predictions Using PANAIR," AIAA Paper 84-2495, 1984.

[18]Maskew, B., "On the Influence of Camber and Non–Planar Vortex Wake on Wing Characteristics in Ground Effects," ARC–CP–1264, 1971.

[19]Chun, H. H., and Park, I. R., "Analysis of Steady and Unsteady Performances for 3-D Air Wings in the Vicinity of the Free Surface," *Proceedings of a Workshop on Twenty-First Century Flying Ships*, edited by L. J. Prandolini, The Inst. of Marine Engineers, Sydney, 1995, pp. 23–46.

[20]Mizutani, N., and Kazuo, S., "Numerical Analysis of 3-D WIG Advancing over the Still Water Surface," *Journal of the Society of Naval Architects of Japan*, Vol. 174, 1993.

[21]Hirata, N., and Kodama, Y., "Flow Computation for Three-Dimensional Wing in Ground Effect Using Multi-Block Technique," Journal of the Society of Naval Architects of Japan, Vol. 177, May 1995, pp. 49–57.

[22]Fink, P. M., and Lastinger, L. J., "Aerodynamic Characteristics of Low-Aspect-Ratio Wings in Ground Proximity to the Ground," NASA TN D-926, May 1961.

[23]Binder, G., "Nonlinear Lifting-Surface Theory for Yawed and Banked Wings in Ground Proximity," *Zhumal Flugwissenschaften und Weltraumforschung*, Vol. 1, No. 4, July 1977, pp. 241–250.

[24]Chang, R. C., "An Experimental Investigation of Dynamic Ground Effect," Ph.D. Dissertation, Aerospace Engineering Dept., Univ. of Kansas, Lawrence, Aug. 1985.

[25]Chang, R. C., and Muirhead, V. U., "Effect of Sink Rate on Ground Effect of Low-Aspect-Ratio Wings," *Journal of Aircraft*, Vol. 24, No. 3, 1987, pp. 176–180.

[26]Lee, P. H., Lan., C. E., and Muirhead, V. H., "An Experimental Investigation of Dynamic Ground Effect," NASA CR-4105, 1987.

[27]Zhang, Xin, and Zerihan, J., "Aerodynamics of a Double-Element Wing in Ground Effect," *AIAA Journal*, Vol. 41, No. 6, 2003, pp. 1007–1016.

[28]Pierson, J., and Helgesen, J., "Tracked Air Cushion Research Vehicle Aerodynamic Analysis," Rept. No. FRA-RT-72-32, PB 212496, 1971.

[29]Eggleton, P. L., and Rudback, N. E., "Advanced Ground Transportation Research Programs in Canada," U.S. DOT Workshop, Sept. 1977.

[30]Kikuchi, K., "Numerical Simulation of the Ground Effect Using the Boundary Element Method," *International Journal for Numerical Methods in Fluids*, Vol. 25, 1997, pp. 1043–1056.

[31]Koh, S. R., Seo, J. H., Moon, Y. J., Cho, J. S., and Yoon, Y. H., "Unsteady Flow and Noise Characteristics of Wing in Ground Effect at Close Proximity," *Proceedings of the Second International Conference on Computational Fluid Dynamics*, 2002.

[32]*Assessment of Experimental Uncertainty with Application to Wind Tunnel Testing*," AIAA, Reston, VA, 1999.

[33]Jang, J.-S. R., "ANFIS: Adaptive-Network-Based Fuzzy Inference Systems," *IEEE Transactions on Systems, Man, and Cybernetics*, Vol. 23, No. 3, 1993, pp. 665–685.

[34]Speyer, J. L., White, J. E., Douglas, R., and Hull, D. G., "Multi-Input/Multi-Output Controller Design for Longitudinal Decoupled Aircraft Motion," *Journal of Guidance, Control, and Dynamics*, Vol. 7, No. 6, 1984.